

Thin- or Thick-Skinned Faulting in the Yakima Fold and Thrust Belt (WA)? Constraints from Kinematic Modeling of the Saddle Mountains Anticline

by Gabriele Casale* and Thomas L. Pratt†

Abstract The Yakima fold and thrust belt (YFTB) deforms the Columbia River Basalt Group flows of Washington State. The YFTB fault geometries and slip rates are crucial parameters for seismic-hazard assessments of nearby dams and nuclear facilities, yet there are competing models for the subsurface fault geometry involving shallowly rooted versus deeply rooted fault systems. The YFTB is also thought to be analogous to the evenly spaced wrinkle ridges found on other terrestrial planets. Using seismic reflection data, borehole logs, and surface geologic data, we tested two proposed kinematic end-member thick- and thin-skinned fault models beneath the Saddle Mountains anticline of the YFTB. Observed subsurface geometry can be produced by 600–800 m of heave along a single listric-reverse fault or ~ 3.5 km of slip along two superposed low-angle thrust faults. Both models require decollement slip between 7 and 9 km depth, resulting in greater fault areas than sometimes assumed in hazard assessments. Both models require initial slip much earlier than previously thought and may provide insight into the subsurface geometry of analogous comparisons to wrinkle ridges observed on other planets.

Introduction

The origin of the Yakima fold and thrust belt (YFTB) of the U.S. Pacific Northwest, a series of anticlinal ridges in eastern Washington and Oregon, has been the subject of extensive debate for nearly a century. The YFTB is a fan-shaped set of asymmetric, anticlinal folds above reverse faults (Fig. 1) extending 150 km in an east–west direction and 100 km in a north–south direction. The folds are intimately associated with the < 5 km thick Columbia River Basalt Group (CRBG) volcanic flows that cover much of eastern Washington State (e.g., Reidel *et al.*, 1989, 1994; Watters, 1989; Campbell and Reidel, 1994). These extensive Miocene basalt flows form a layered sequence that has been faulted and folded to form the anticlines.

There is a long-standing debate whether the YFTB formed by thin-skinned thrusting, in which the faults sole into a detachment at the base of the CRBG flows at 5 km depth or less (e.g., Reidel *et al.*, 1989, 1994; Watters, 1989; Campbell and Reidel, 1994), or by thick-skinned thrusting, in which the faults reach the middle crust (e.g., Montgomery, 2008; Blakely *et al.*, 2011; Pratt, 2012). Potential-field mod-

eling and continuation of YFTB faults west of the CRBG suggest the faults penetrate below the basalts (Campbell, 1989; Blakely *et al.*, 2011), but definitive evidence is lacking and seismicity does not delineate the fault geometry (Gomberg *et al.*, 2012).

Understanding YFTB structures is of more than local interest. The YFTB fault geometries and slip rates are critical parameters for assessing seismic hazards for major dams on the Columbia and Snake Rivers and for the Hanford nuclear site, which contains the nation's largest collection of high-level radioactive waste (Geomatrix Consultants, 1996; Benjamin and Associates *et al.*, 2012). Estimated maximum magnitudes of earthquakes on YFTB structures range from M_w 5.2 to 7.8 for different fault geometries inferred from indirect observations such as projection of distant features (e.g., Tabor *et al.*, 1984; Price and Watkinson, 1989; Cheney and Hayman, 2009).

Perhaps the best studied YFTB structure is the Saddle Mountains anticline (SMA) (Fig. 1), which is a hanging-wall fold above a south-dipping reverse fault (Reidel, 1984, 1988; Campbell, 1989). The timing of onset of slip on the SMA fault is unknown, but thinning of the Grand Ronde Basalt (17–15.6 Ma) over the SMA requires uplift to have begun by at least middle Miocene (Reidel, 1984). Onlapping of later CRBG flows record continued anticlinal growth through late

*Now at Department of Geology, Appalachian State University, ASU Box 32067, Boone, North Carolina 28608-2067.

†Now at U.S. Geological Survey, MS 905, 12201 Sunrise Valley Drive, Reston, Virginia 20192.

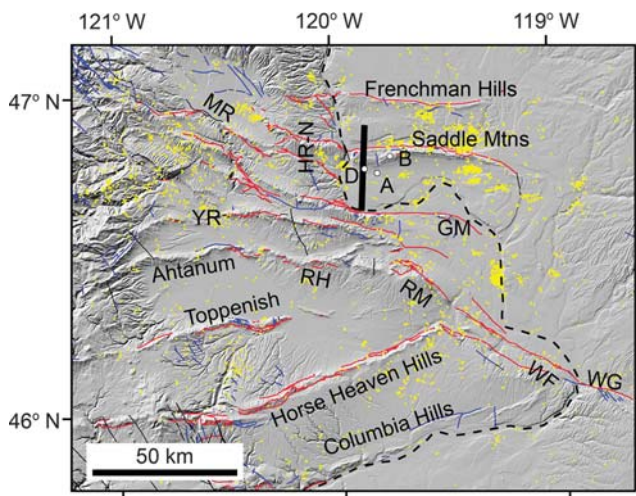


Figure 1. Shaded relief map of the Yakima fold and thrust belt showing the approximate location of the seismic profile (bold black line). MR, Manastash ridge; UR, Umtanum ridge; YR, Yakima ridge; RH, Rattlesnake Hills; RM, Rattlesnake Mountain; WF, Wallula fault; WG, Wallula Gap; and GM, Gable Mountain. White dots show drillhole locations: A, Anderville Farms #1A; B, BN 1-9; and D, DH-5. Thrust faults (red line), normal faults (blue lines), and strike-slip faults (thin black lines) from the U.S. Geological Survey (USGS) Quaternary fault and fold database and the Washington State Department of Natural Resources 1:100,000 geologic map database (see [Data and Resources](#)). Dashed black line shows the Columbia River.

Miocene time (15.6–8.5 Ma; [Reidel, 1984](#); [Reidel et al., 1989, 1994](#)), and post-CRBG uplift of the SMA displaces the late Miocene and early Pliocene fluvial Ringold Formation (8.5–3.5 Ma) by ~400 m above the modern Columbia River flood plain ([Reidel, 1984, 1988](#)). Modern motion on YFTB faults is shown by deformation of late Quaternary deposits ([Campbell and Bentley, 1981](#); [West et al., 1996](#); [Blakely et al., 2011](#)), geodetically observed active shortening ([McCaffrey et al., 2013](#)), and active seismicity ([Gomberg et al., 2012](#)).

The legacy of alternative models of sub-SMA fault geometry is illustrative of the persistent thick- versus thin-skinned debate in the YFTB. [Reidel et al. \(1989\)](#) used borehole chemical and geophysical logs to infer a shallow fault dip, and presumably a shallow decollement, beneath the SMA from a repeated section in the BN 1-9 borehole (Fig. 1) bounded below by a low-resistivity zone interpreted as a brecciated fault zone (S. Reidel, written comm., 2012). A reverse fault that extends through the brecciated zone and reaches the surface at the north edge of the SMA suggests a dip of ~32° south. Alternatively, this fault may be a splay off a steeper reverse fault that was not penetrated by the BN 1-9 borehole ([Reidel et al., 1989](#)). In contrast, potential field modeling is consistent with more steeply dipping, deeply penetrating faults forming the YFTB anticlines ([Blakely et al., 2011](#)).

Seismic reflection profiles rarely see below the CRBG strata, but here we present a seismic profile that images fold-

ing in rocks at 7 km depth beneath the SMA and below the base of the CRBG (Fig. 2). Using the geometry of the strata imaged on this seismic profile, we explore the two end-member kinematic models often proposed for formation of YFTB structures: (1) a thin-skinned model in which the shallow dipping thrust fault forming the SMA soles into a shallow detachment near the estimated depth to the base of the CRBG and (2) a thick-skinned model consisting of a steep reverse fault penetrating to depths well below the CRBG. In our study, we assess the fault geometry necessary to make each model viable and examine the implications of the end-member models. Our results not only constrain the crustal structure and fault geometry in the YFTB but also place limits on the timing of fold initiation.

The YFTB structures also have been cited as analogs for curious, often evenly spaced wrinkle ridges on other terrestrial planets, which has sparked debate about the origin, depth of faulting, and controls on ridge spacing ([Watters, 1989, 1991, 1992](#); [Mangold et al., 1998](#); [Mège and Reidel, 2001](#); [Montési and Zuber, 2003](#); [Mueller and Golombek, 2004](#)). Our results have implications for the use of the YFTB structures as analogs for planetary ridges, and may inform future investigations into these planetary tectonic features.

Seismic Reflection Data

The seismic profile across the SMA is a proprietary line purchased by the U.S. Geological Survey (USGS) with limited publication rights. The CRBG form notoriously difficult terrain in which to carry out subsurface imaging, and the profile is one of few in the region that shows reflectivity below a few kilometers depth. The profile was collected with vibrator sources, and the finished profile has a 46 m trace spacing. We reprocessed the data using an extended correlation technique ([Okaya and Jarchow, 1989](#)) to image to 10 km depth. The processing was routine but made use of multiple applications of residual statics analyses alternating with velocity analyses. Despite these extensive acquisition and processing efforts, subsurface reflections remained weak. Because of the layered nature of the CRBG, the processing steps included deconvolution to reduce multiply reflected energy. This was an important step in the processing, and the autocorrelations of the processed data did not show obvious peaks indicative of multiples on the finished seismic profile. The stacked data were frequency–wavenumber analysis ($f-k$) migrated and converted to depth using smoothed stacking velocities. The subsurface velocities reached about 4 km/s within the upper 2 km, which is consistent with shallow or exposed basalt flows beneath the profile. The stacking velocities are not well constrained because of the weak reflectivity, and the depth calculations are, therefore, estimated to potentially have errors of 10%–15%. The topographic profile was extracted from publicly available Shuttle Radar Topography Mission data (see [Data and Resources](#)).

The SMA fault was not directly imaged by the seismic profile, so our modeling relied on the geometric relationships

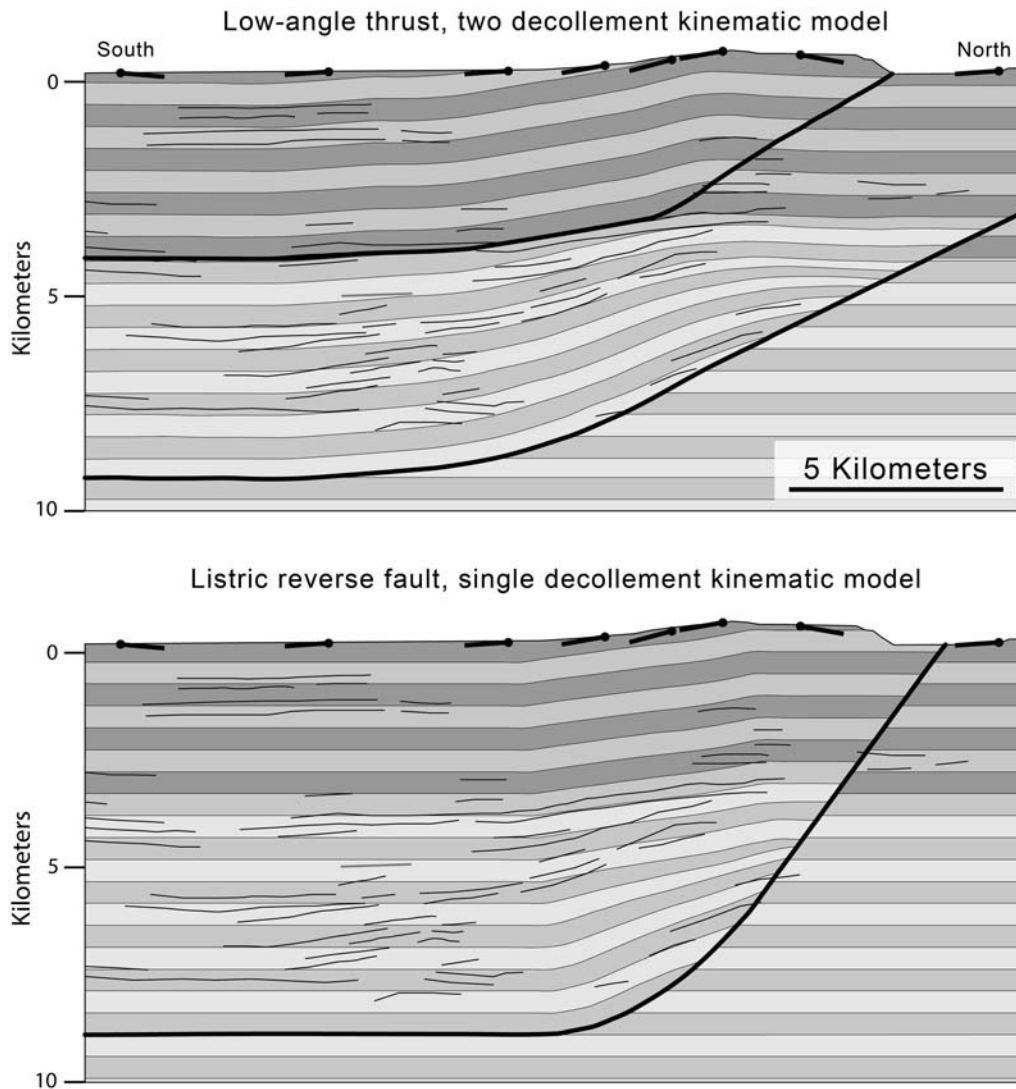


Figure 2. Seismic reflection profile with approximate locations of projected boreholes (top) and interpreted seismic reflection profile (bottom). Line thickness indicates relative interpretation confidence; discernible geometric relationships described in the text are labeled. The extent of the models in Figure 3 is shown along the bottom. The cross sections have no vertical exaggeration. Seismic data are owned or controlled by Seismic Exchange, Inc. (see [Data and Resources](#)); interpretation is that of the USGS.

between stratal units interpreted from the seismic profile (Fig. 2). Two boreholes in the vicinity of the SMA penetrated the CRBG strata: the BN 1-9 drillhole near the crest of the anticline and the Anderville Farms #1A (AF-1A) drillhole south of the anticline. A third borehole DH-5 penetrated into the basalts on the backlimb of the anticline. The AF-1A borehole intersection with the base of the CRBG at about 4 km depth coincides with a continuous, relatively strong reflector showing little dip near the borehole south of the anticline but arched upward within the anticline. South of the SMA, reflectors are subhorizontal to 7–8 km depth, but gently south dipping reflectors ($\sim 7^\circ$) are imaged in the southern limb of the SMA. These subsurface reflector attitudes match basalt flow attitudes mapped at the surface (Fig. 2; Reidel, 1984, 1988). From the crest of the anticline north, reflector segments are nearly horizontal.

Unfortunately, the steep topography on the north side of the anticline prevented access for collection of the seismic reflection data, resulting in an area of missing or low-fold data north of the anticline's crest. This key area includes the near-surface portion of the thrust fault, precluding an interpretation of the dip and precise location of the fault based on the seismic profile.

No discrete axial hinge separates the regions of horizontal and inclined reflectors within or south of the anticline; instead, this change occurs over several kilometers in a diffuse axial hinge zone. Between 5 and 8 km depth, the inclination of the south-dipping reflectors directly beneath the SMA increases from $\sim 12^\circ$ to $\sim 20^\circ$, respectively. We interpret this change in reflector dip as marking tapered bedding indicative of syn-tectonic onlapping. These relationships demonstrate fold growth before and during deposition of the CRBG strata.

Kinematic Modeling Methodology and Limitations

Kinematic models have long been utilized to study fault-related folding (e.g., [Suppe, 1983](#); [Suppe and Medwedeff, 1990](#); [Wilkerson *et al.*, 1991](#)), and flexural slip-based models are useful for inferring fault geometry from folding of stratified rocks (e.g., [Suppe, 1983](#); [Savage and Cooke, 2003](#)). We used the stratigraphic and geometric fold relationships within the SMA discerned from the seismic profile, published borehole data (see [Data and Resources](#)), and surface observations ([Reidel, 1988](#); [Reidel and Fecht, 1994](#)) to constrain the kinematic models. We tested the two commonly proposed end-member models (thin- and thick-skinned faulting) by iterative kinematic forward modeling to make balanced, restorable cross sections of the SMA. We selected starting fault geometries for each fault style and then progressively modified these models to make the deformed cross sections match the observed geometry of strata within the SMA.

There are a number of kinematic algorithms commonly used to model fault geometries and associated fold structures ([Shaw *et al.*, 2005](#)), including fault propagation folding ([Suppe and Medwedeff, 1990](#)), trishear ([Erslev, 1991](#); [Allmendinger, 1998](#)), inclined shear ([Gibbs, 1983](#); [Buddin *et al.*, 1997](#)), fault-parallel flow ([Sanderson, 1982](#)), and fault-bend folding ([Suppe, 1983](#)). Here, we use the fault-bend fold algorithm because it accommodates hanging-wall deformation via flexural slip, which is supported in the CRBG region by field observations of bedding-parallel slip scarps ([Price and Watkinson, 1989](#); [Blakely *et al.*, 2011](#)). Steeply dipping hanging-wall reflectors along the fault, the hallmark of trishear and fault propagation folding, are not observed at the spatial resolution of our seismic reflection profile or in the surface geology. The absence of an inclined hanging-wall forelimb implies that either fault propagation dramatically exceeds fault slip or the apical angle of the fault-tip deformation zone is narrow. Therefore, these latter two kinematic models would produce virtually identical results to fault-bend folding.

The aim of this article is to inform the ongoing debate about the angle and depth of penetration of Yakima fold sub-jacent faulting. We, therefore, restricted our models to the most simplistic fault geometries that describe the geometric features observed in the seismic profile. In some cases, the simplicity of our models comes at the expense of accuracy but does not greatly modify our estimates of timing and total slip. Moreover, our models address only the dip-slip component of motion on the faults, although the possibility of strike-slip motion on YFTB structures has been debated (e.g., [Reidel *et al.*, 1989, 1994](#); [Pratt, 2012](#)). An oblique component of motion would increase the total slip on the faults, but our analysis of the dip-slip component would not be affected substantially because the along-strike variation in surface uplift of the SMA is below the resolution of our models.

Results

Model 1: Low-angle Thrust Fault

Our first model tests the thin-skinned, low-angle thrust fault interpretation for the YFTB folds. In this model, the thrust fault dips at 35° or less and soles into a subhorizontal decollement at the base of the CRBG at about 4 km depth. The implication of this model from a hazard assessment perspective is the decollement at the base of the CRBG lies at a large contrast in rock types at the top of weak sedimentary strata, resulting in the seismic moment during earthquakes being concentrated within the dipping fault plane where it cuts the CRBG. This effectively limits the maximum earthquake magnitudes to about 6.5.

Low-angle faulting beneath the SMA with a decollement horizon at the base of the CRBG reproduces the observed surface geometry with 350–450 m of heave (Fig. 3a). However, to reproduce the observed sub-CRBG deformation, specifically the onlapping reflectors and steeper dips of strata beneath the anticline, requires a second fault with a ramp soling into a decollement at 8–9 km. The necessity of this latter fault argues that faults can only locally follow the thin-skin model beneath the anticlines; deeper faults that violate the thin-skin model must extend into the sub-CRBG strata. Because the anticline in the sub-CRBG strata coincides with the anticline at the surface and therefore appears to be related, the deeper fault cannot be considered an older, inactive fault that pre-dates the Miocene CRBG flows.

Synconvergence deposition of pre-CRBG sediments is necessary to account for tapered bedding observed on the seismic profile along the lower ramp, with decreasing total heave reflected in younger, up-section folds. The separation of the deepest beds across the lower fault requires a minimum 7.6 km of heave on the lower fault, with about 3.2 km after deposition of the CRBG. The folds formed by the upper and lower faults can be independent structures, but they also could be related by interaction between the structures. The deeper fault extends north of the SMA in our model, perhaps forming the Frenchman Hills anticline to about 18 km north (Fig. 1). To the south, the faults presumably merge with faults forming Umtanum ridge (Gable Mountain) and other structures (e.g., [Pratt, 2012](#)).

Model 2: Thick-Skin, Listric-Reverse Fault

Folding beneath the SMA can alternatively be accounted for by slip along a single listric-reverse fault soling into a decollement at 7–9 km deep (Fig. 3b). Because the decollement lies in the strata well below the base of the CRBG, this model is often considered the thick-skin alternative. The upper portion of the fault in this model dips at about 54° and is consistent with the interpretation of an absence of a fault cutting the BN 1-9 borehole ([Reidel *et al.*, 1989](#)). Similar to the thin-skinned model, tapered bedding below the SMA crest is accounted for by onlapping of synconvergence, pre-CRBG sediments. Inclination of the deepest beds requires

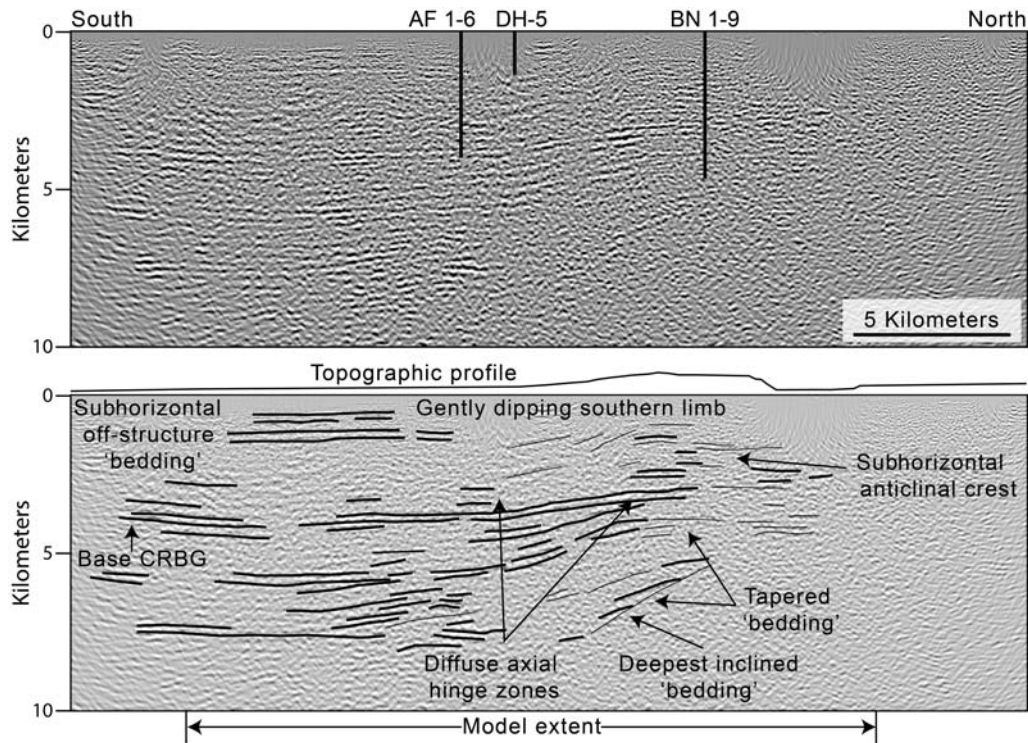


Figure 3. Kinematic models for the Saddle Mountains anticline. (Top) Thin-skinned model showing the anticline within the Columbia River Basalt Group (CRBG) being formed from a combination of a shallow dipping ($\sim 30^\circ$) thrust fault above a deeper fault responsible for the folding of the deeper strata. (Bottom) Thick-skinned listric-reverse fault model in which the fault curvature is responsible for the broad, shallow dipping backlimb. Projected bedding attitudes shown as bold black ticks along the topographic profile are from the Washington State Department of Natural Resources 1:100,000 geologic map database (see [Data and Resources](#)) The cross sections have no vertical exaggeration.

at least 2 km of decollement heave to transport the beds along the curved portion of the fault, of which ~ 600 – 800 m occurs after emplacement of the CRBG.

Given a steep fault dip, the relatively shallow inclination of the SMA backlimb must reflect a listric-fault geometry at depth. The dips of the strata in the backlimb of the SMA nowhere exceed 20° – 30° and are typically 10° or less (Fig. 2; [Reidel, 1984](#)). Relating the backlimb dip to fault curvature produces gently inclined backlimbs in folds formed by steeply dipping faults (e.g., [Erslev, 1986](#)), provided that total heave does not exceed the length of the curved and inclined ramp. The fault curvature is constrained to a minimum depth of ~ 7 km by the deepest inclined reflectors and a maximum depth of about 9 km by the lateral extent of inclined beds at the surface.

The thick-skinned listric-fault model has two major limitations not shared by the thin-skinned model. First, to include deep inclined reflectors into the hanging wall, the fault must intersect the surface several hundred meters north of the topographic expression of the SMA. No surface observations exist to accurately determine the location of surface rupture of the SMA fault, and fluvial sediments located along the margin of the SMA indicate that erosion may have back-cut the original topographic expression of anticlinal uplift. Nonetheless, extant geologic maps place the concealed fault

trace along the margin of the SMA ([Reidel, 1988](#)), contrary to the thick-skinned model presented here. Second, the thick-skinned model does not accurately account for the deepest inclined reflectors in the sub-CRBG backlimb of the fold. A synthetic fault splay rooted in the subhorizontal detachment surface that ceased to be active prior to deposition of the CRBG could explain the inclination of these deepest reflectors. Timing and near-fault total slip were determined using the near-fault reflectors in the deepest part of the section and the base-CRBG reflectors and surface geometry in the shallow part of the section; therefore, the presence or absence of this ancillary fault would not modify our results.

Discussion

Sub-CRBG strata with significantly steeper dips than the overlying CRBG indicates that anticlinal growth began before deposition of the CRBG. The sub-CRBG rocks have been interpreted as late Eocene to early Miocene synextension sediments deposited in fault-bounded grabens ([Cashman and Whetten, 1976](#); [Catchings and Mooney, 1988](#); [Taylor et al., 1988](#); [Campbell, 1989](#); [Evans, 1994](#)) or in synclinal basins between reverse faults ([Cheney and Hayman, 2009](#)). Tapered bedding of the sub-CRBG strata (Fig. 2) indicates onlapping

on a growing anticlinal structure, which implies the shortening dates to as early as late Eocene time.

Our kinematic models provide estimates of long-term fault-slip rates, which are a primary factor in seismic-hazard assessments (Geomatrix Consultants, 1996; Benjamin and Associates *et al.*, 2012). In our thick-skinned model, we interpret ~600–800 m of total decollement heave following middle and late Miocene deposition of the CRBG, whereas in our thin-skinned model about 350–450 m of post-CRBG heave is required on the upper fault. These estimates result in post-CRBG average slip rates of about 0.07–0.09 mm/yr for the deep listric fault and 0.04–0.05 mm/yr for the upper of the shallowly dipping faults. These rates are at the low end of previous estimates (e.g., Benjamin and Associates *et al.*, 2012). The ~3.2 km of post-CRBG slip on the deeper fault in our thin-skinned model, however, produces a much higher slip rate of 0.4 mm/yr. The amount of slip needed on the upper fault in our thin-skinned model or the listric fault in our thick-skinned model to lift the Ringold Formation (after 3.5 Ma), which is a fluvial deposit found on the crest of the SMA (Reidel, 1984), from the base of the anticline results in higher slip rates in the 0.10–0.23 mm/yr range. These latter rates are at the high end of recent estimates made for hazard assessments (e.g., Benjamin and Associates *et al.*, 2012).

The maximum earthquake magnitudes used in hazard assessments are directly influenced by fault geometry (Geomatrix Consultants, 1996; Benjamin and Associates *et al.*, 2012). Lacking constraints on fault geometry, past hazard assessments have treated the faults as planar surfaces with a variety of possible dip angles (15°–60°) and maximum depths (fault widths) of 2.5–22 km. The variable fault areas result in a broad range of maximum earthquake magnitudes (M_w 5.2–7.7 for the SMA). Our models have different geometries and depths from the simple planar faults assumed in the hazard assessments and include subhorizontal decollements that were not explicitly included in past hazard assessments. The relatively large fault areas in our models, compared with previous estimates for thin-skin models in which the seismogenic portion of the fault is limited to the dipping portion within the CRBG, therefore suggest the maximum magnitudes could be consistent with the larger maximum magnitudes from thick-skin models considered in earlier hazard assessments. We do not know the extent of the faults to the south of our models, however, so precise estimates of maximum magnitudes remain elusive.

Are there ways to test the models? One difference between the models is that the thin-skinned model allows for (but does not require) the fault to reach the surface along the north edge of the uplift (Fig. 3). In contrast, the surface location of the thrust fault in the thick-skinned model is north of the SMA, implying that either the north edge of the anticline topography has been eroded or the fault would need to steepen in the near-surface to bring it nearer the topographic front. Excavations of the shallow portions of the fault could give insights into its location and dip. Another potential test is by compatibility and/or analogy with other YFTB struc-

tures. Our kinematic models place specific limits upon the faults such as depth to decollement, fault curvature, and radius. Many of these features are constrained by the geometry of the upper basalt layers and topography. Other YFTB structures presumably have a similar style of folding, and modeling these other structures could provide additional constraints that favor one or the other style of faulting.

The Yakima folds form the basis of some kinematic and geometric models of analog wrinkle ridge structures on other terrestrial planets (Watters, 1991, 1992, 2004; Mège and Ernst, 2001; Mège and Reidel, 2001). Watters (1989, 1991) argued the Yakima folds, and by inference Martian wrinkle ridges, can be modeled by buckling of an elastic beam (CRBG) above a relatively weak medium (sub-CRBG sedimentary rocks). Mège and Reidel (2001) suggested the relationship between shortening and ridge length in the YFTB may serve as a proxy to quantify shortening within Martian wrinkle ridges based on ridge length. Our kinematic models demonstrate that surface morphology is not solely the result of postdepositional fault slip that is decoupled from underlying strata. The pre-CRBG initiation of folding requires that aspects of the YFTB geometry, specifically spacing, were established prior to emplacement of the CRBG. In this respect, our kinematic models favor deeper-penetrating faults, which suggests that Martian wrinkle ridge spacing is a function of lithospheric thickness (e.g., Montési and Zuber, 2003; Mueller and Golombek, 2004).

Other authors have used inversion of Mars Orbiter Laser Altimeter topography data across wrinkle ridges and other Martian structures (e.g., Amenthes Rupes) to determine fault geometry at depth (e.g., Schultz and Watters, 2001; Okubo and Schultz, 2004; Mueller *et al.*, 2014). In the absence of erosion, topography serves as an individual horizon; the dual models presented here provide an example of the range of suitable geometric configurations and total slip values that adequately fit a set of deformed horizons. Okubo and Schultz (2004) used inferred subjacent fault geometry as a proxy for the distribution of mechanical heterogeneity in the Martian crust. Although their results were focused primarily on the presence or absence of back thrusting, their overall fault geometries in general bear striking resemblance to our models, including superposed detachment surfaces and concave-up listric thrust faulting. Moreover, these authors argue that certain geometric aspects of Martian wrinkle ridges are the result of mechanical heterogeneity; there is likely a pronounced mechanical contrast between the CRBG and underlying sedimentary rocks in the Yakima fold and thrust belt. These mechanical and geometric similarities support the notion that in some respects the Yakima folds are suitable terrestrial proxies for planetary wrinkle ridges and may provide some insight into the subsurface structure, crustal configuration, frictional properties, and large-scale strain on other planets.

Conclusions

We present a seismic reflection profile showing folding of sub-CRBG strata beneath the SMA, and we test proposed

kinematic models of high- and low-angle faults to see what fault geometries are needed in these models to satisfy observed geometric relationships. We emphasize three main conclusions: (a) soling of the fault beneath the SMA into a decollement horizon is necessary to satisfy kinematic constraints; (b) the SMA has had 350–800 m of post-CRBG fault slip, and perhaps post-Ringold (~3.5 Ma) slip, depending on the fault geometry; (c) shortening within the YFTB was active during deposition of the sub-CRBG Eocene and Oligocene strata. The models presented here should be considered representative, and the interpretive latitude is illustrated by the significant geometric contrasts between our two models. Similar modeling of other YFTB structures may be an effective way to test models for the formation of the entire YFTB system and for similar tectonic features observed on other planetary bodies.

Data and Resources

The seismic reflection profile used in this article is proprietary and is available for purchase from Seismic Exchange, Inc. The interpretation is solely the responsibility of the authors. Borehole logs and surface geologic information used as constraints for the subsurface interpretation include Washington State 1:100,000 geologic maps, Shell Oil Co., BN 1-9; Sierra Geophysics and Rockwell Hanford Operations, DH-5; Delta Petroleum Corporation, Andersonville Farms 1-6. These data are publicly available and can be accessed at www.dnr.wa.gov (last accessed August 2014). Additional surface geologic information shown in Figure 1 comes from the U.S. Geological Survey (USGS) Quaternary fault and fold database (<http://earthquake.usgs.gov/hazards/qfaults/>; last accessed August 2014). Void filled 1 arcsec Shuttle Radar Topography Mission elevation data shown in Figure 1 and used to construct the topographic profiles in Figures 2 and 3 is publicly available from the <https://ita.cr.usgs.gov> (last accessed December 2014).

Acknowledgments

The modeling was carried out using Midland Valley's 2DMOVE software. We thank Seismic Exchange, Inc. for allowing us to publish the seismic profile. The manuscript has benefited from discussions with Steve Reidel, Rick Blakely, and Brian Sherrod, and reviews by Anne Egger, Juliet Crider, Kelvin Berryman, Karl Mueller, and an anonymous reviewer.

References

Allmendinger, R. W. (1998). Inverse and forward numerical modeling of trishear fault-propagation folds, *Tectonics* **17**, no. 4, 640–656.

Benjamin and Associates, URS Corporation, Geomatrix Consultants, and Shannon & Wilson (2012). *Probabilistic Seismic Hazard Analyses Project for the mid-Columbia Dams*, Prepared for Public Utilities Districts of Chelan, Douglas, and Grant Counties, 344 pp.

Blakely, R. J., B. L. Sherrod, C. S. Weaver, R. E. Wells, A. C. Rohay, E. A. Barnett, and N. E. Knepprath (2011). Connecting the Yakima fold and thrust belt to active faults in the Puget Lowland, Washington, *J. Geophys. Res.* **116**, no. B07105, doi: [10.1029/2010JB008091](https://doi.org/10.1029/2010JB008091).

Buddin, T. S., S. J. Kane, G. D. Williams, and S. S. Egan (1997). A sensitivity analysis of 3-dimensional restoration techniques using vertical and inclined shear constructions, *Tectonophysics* **269**, nos. 1/2, 33–50.

Campbell, N. P. (1989). Structural and stratigraphic interpretation of rocks under the Yakima fold belt, Columbia Basin, based on recent surface mapping and well data, in *Volcanism and Tectonism in the Columbia River Flood-Basalt Province*, Geological Society of America Special Paper, S. P. Reidel and P. R. Hooper (Editors), Vol. 239, Geological Society of America, Boulder, Colorado, 209–222.

Campbell, N. P., and R. D. Bentley (1981). Late Quaternary deformation of the Toppenish Ridge uplift in south-central Washington, *Geology* **9**, 519–524.

Campbell, N. P., and S. P. Reidel (1994). Further exploration for gas warranted in Columbia basin, *Oil Gas J.* **92**, 127–132.

Cashman, S. M., and J. T. Whetten (1976). Low-temperature serpentinization of peridotite fanglomerate on the west margin of the Chiwaukum graben, Washington, *Geol. Soc. Am. Bull.* **87**, 1773–1776.

Catchings, R., and W. Mooney (1988). Crustal structure of the Columbia plateau: Evidence for continental rifting, *J. Geophys. Res.* **93**, 459–474.

Cheney, E. S., and N. Hayman (2009). The Chiwaukum structural low: Cenozoic shortening of the central Cascade range, Washington State, USA, *Geol. Soc. Am. Bull.* **121**, 1135–1153.

Erslev, E. A. (1986). Basement balancing of Rocky Mountain foreland uplifts, *Geology* **14**, 259–262.

Erslev, E. A. (1991). Trishear fault-propagation folding, *Geology* **19**, no. 6, 617–620.

Evans, J. E. (1994). Depositional history of the Eocene Chumstick Formation: Implications of tectonic partitioning for the history of the Leavenworth and Entiat-Eagle Creek fault systems, Washington, *Tectonics* **13**, 1425–1444.

Geomatrix Consultants (1996). *Probabilistic Seismic Hazard Analysis DOE Hanford Site*, Washington, WHC-SD-W236A-TI-002, Rev. 1, 372 pp., <http://pdw.hanford.gov/arpir/pdf.cfm?accession=D196005995> (last accessed December 2014).

Gibbs, A. D. (1983). Balanced cross-section construction from seismic sections in areas of extensional tectonics, *J. Struct. Geol.* **5**, no. 2, 153–160.

Gomberg, J., B. Sherrod, M. Trautman, E. Burns, and D. Snyder (2012). Contemporary seismicity in and around the Yakima fold and Thrust belt in eastern Washington, *Bull. Seismol. Soc. Am.* **102**, 309–320.

Mangold, N., P. Allemand, and P. G. Thomas (1998). Wrinkle ridges of Mars: Structural analysis and evidence for shallow deformation controlled by ice-rich decollements, *Planet. Space Sci.* **46**, 345–356.

McCaffrey, R., R. W. King, S. J. Payne, and M. Lancaster (2013). Active tectonics of northwestern U.S. inferred from GPS-derived surface velocities, *J. Geophys. Res.* **118**, 1–15, doi: [10.1029/2012JB009473](https://doi.org/10.1029/2012JB009473).

Mège, D., and R. E. Ernst (2001). Contractual effects of mantle plumes on Earth, Mars, and Venus, *Geol. Soc. Am. Spec. Pap.* **352**, 103–140.

Mège, D., and S. P. Reidel (2001). A method for estimating 2D wrinkle ridge strain from application of fault displacement scaling to the Yakima folds, Washington, *Geophys. Res. Lett.* **28**, 3545–3548.

Montési, L. G. J., and M. T. Zuber (2003). Clues to the lithospheric structure of Mars from wrinkle ridge sets and localization instability, *J. Geophys. Res.* **108**, 1–25.

Montgomery, S. L. (2008). New exploration concepts highlight Columbia River basin's potential, *Oil Gas J.* **106**, 35–42.

Mueller, K., and M. Golombek (2004). Compressional structures on Mars, *Annu. Rev. Earth Planet. Sci.* **32**, 435–464, doi: [10.1146/annurev-earth.32.101802.120553](https://doi.org/10.1146/annurev-earth.32.101802.120553).

Mueller, K., A. Vidal, S. Robbins, M. Golombek, and C. West (2014). Fault and fold growth of the Amenthes uplift: Implications for Late Noachian crustal rheology and heat flow on Mars, *Earth Planet. Sci. Lett.* **408**, 100–109.

Okaya, D. A., and C. M. Jarchow (1989). Extraction of deep crustal reflections from shallow Vibroseis data using extended correlation, *Geophysics* **54**, 555–562.

Okubo, C. H., and R. A. Schultz (2004). Mechanical stratigraphy in the western equatorial region of Mars based on thrust fault-related fold

- topography and implications for near-surface volatile reservoirs, *Geol. Soc. Am. Bull.* **116**, nos. 5/6, 594–605.
- Pratt, T. L. (2012). Large-scale splay faults on a strike-slip fault system: The Yakima folds, Washington State, *Geochem. Geophys. Geosyst.* **13**, Q11004, doi: [10.1029/2012GC004405](https://doi.org/10.1029/2012GC004405).
- Price, E. H., and A. J. Watkinson (1989). Structural geometry and strain distribution within eastern Umtanum fold ridge, south-central Washington, in *Volcanism and Tectonism in the Columbia River Flood-Basalt Province, Geological Society of America Special Paper*, S. P. Reidel and P. R. Hooper (Editors), Vol. 239, Geological Society of America, Boulder, Colorado, 265–281.
- Reidel, S. P. (1984). The Saddle Mountains; the evolution of an anticline in the Yakima fold belt, *Am. J. Sci.* **284**, 942–978.
- Reidel, S. P. (1988). Geologic map of the Saddle Mountains, south-central Washington, *Washington Division of Geology and Earth Resources Geologic Map GM-38, 5 plates*, scale 1:48,000, 28 pp.
- Reidel, S. P., and K. R. Fecht (1994). Geologic map of the Priest Rapids 1:100,000 quadrangle, *Washington Division of Geology and Earth Resources Open-File Rept. 94-13*, 1 plate, 22 pp., http://www.dnr.wa.gov/Publications/ger_of94-13_geol_map_priestrapids_100k.zip (last accessed December 2014).
- Reidel, S. P., N. P. Campbell, K. R. Fecht, and K. A. Lindsey (1994). Late Cenozoic structure and stratigraphy of south-central Washington, in *Regional Geology of Washington State, Washington Division of Geology and Earth Resources Bulletin*, R. Lasmanis and E. S. Cheney (Editors), Vol. 80, Washington Division of Geology and Earth Resources, Olympia, Washington, 159–180.
- Reidel, S. P., K. R. Fecht, M. C. Hagood, and T. L. Tolan (1989). The geologic evolution of the central Columbia plateau, in *Volcanism and Tectonism in the Columbia River Flood-Basalt Province, Geological Society of America Special Paper*, S. P. Reidel and P. R. Hooper (Editors), Vol. 239, Geological Society of America, Boulder, Colorado, 247–264.
- Sanderson, D. J. (1982). Models of strain variation in nappes and thrust sheets: A review, *Tectonophysics* **88**, no. 3, 201–233.
- Savage, H. M., and M. L. Cooke (2003). Can flat-ramp-flat fault geometry be inferred from fold shape?: A comparison of kinematic and mechanical folds, *J. Struct. Geol.* **25**, 2023–2034.
- Schultz, R. A., and T. R. Watters (2001). Forward mechanical modeling of the Amenthes Rupes thrust fault on Mars, *Geophys. Res. Lett.* **28**, no. 24, 4659–4662.
- Shaw, J. H., C. Connors, and J. Suppe (Editors) (2005). *Seismic Interpretation of Contractional Fault-Related Folds*, American Association of Petroleum Geologists, Tulsa, Oklahoma, Studies in Geology #53, 157 pp.
- Suppe, J. (1983). Geometry and kinematics of fault-bend folding, *Am. J. Sci.* **283**, 684–721.
- Suppe, J., and D. A. Medwedeff (1990). Geometry and kinematics of fault-propagation folding, *Eclogae Geol. Helv.* **83**, 409–454.
- Tabor, R., V. Frizzell Jr., J. Vance, and C. Naeser (1984). Ages and stratigraphy of lower and middle Tertiary sedimentary and volcanic rocks of the central Cascades, Washington: Application to the tectonic history of the Straight Creek fault, *Geol. Soc. Am. Bull.* **95**, 26–44.
- Taylor, S. B., S. Y. Johnson, G. T. Fraser, and J. W. Roberts (1988). Sedimentation and tectonics of the lower and middle Eocene Swauk formation in eastern Swauk Basin, central Cascades, central Washington, *Can. J. Earth Sci.* **25**, 1020–1036.
- Watters, T. R. (1989). Periodically spaced anticlines of the Columbia plateau, in *Volcanism and Tectonism in the Columbia River Flood-Basalt Province, Geological Society of America Special Paper*, S. P. Reidel and P. R. Hooper (Editors), Vol. 239, Geological Society of America, Boulder, Colorado, 283–292.
- Watters, T. R. (1991). Origin of periodically spaced wrinkle ridges on the Tharsis plateau of Mars, *J. Geophys. Res.* **96**, 15.
- Watters, T. R. (1992). System of tectonic features common to Earth, Mars, and Venus, *Geology* **20**, 609–612.
- Watters, T. R. (2004). Elastic dislocation modeling of wrinkle ridges on Mars, *Icarus* **171**, no. 2, 284–294.
- West, M., F. Ashland, A. Busacca, G. Berger, and M. Shaffer (1996). Late Quaternary deformation, Saddle Mountains anticline, south-central Washington, *Geology* **24**, 1123–1126.
- Wilkerson, S. M., D. A. Medwedeff, and S. Marshak (1991). Geometrical modeling of fault-related folds: A pseudo-three-dimensional approach, *J. Struct. Geol.* **13**, 801–812.

Department of Earth and Space Sciences
University of Washington
Johnson Hall Room 070
Box 351310
4000 15th Avenue NE
Seattle, Washington 98195-1310
casalegm@appstate.edu
(G.C.)

U.S. Geological Survey
School of Oceanography
University of Washington
Marine Sciences Building, Room G
1501 NE Boat Street
Seattle, Washington 98195
tpratt@usgs.gov
(T.L.P.)

Manuscript received 23 February 2014;
Published Online 27 January 2015